52,000 years of woolly rhinoceros population dynamics reveal extinction mechanisms

Damien A. Fordham[a,b,c,1], Stuart C. Brown[a,d], Elisabetta Canteri[a,b], Jeremy J. Austin[a], Mark V. Lomolino[e], Sean Haythorne[a,f], Edward Armstrong[g], Hervé Bocherens[h,i], Andrea Manica[j], Alba Rey-Iglesia[d], Carsten Rahbek[b,c,k,l], David Nogués-Bravo[b], and Eline D. Lorenzen[d]

The extinction of the woolly rhinoceros (*Coelodonta antiquitatis*) at the onset of the Holocene remains an enigma, with conflicting evidence regarding its cause and spatiotemporal dynamics. This partly reflects challenges in determining demographic responses of late Quaternary megafauna to climatic and anthropogenic causal drivers with available genetic and paleontological techniques. Here, we show that elucidating mechanisms of ancient extinctions can benefit from a detailed understanding of fine-scale metapopulation dynamics, operating over many millennia. Using an abundant fossil record, ancient DNA, and high-resolution simulation models, we untangle the ecological mechanisms and causal drivers that are likely to have been integral in the decline and later extinction of the woolly rhinoceros. Our 52,000-y reconstruction of distribution-wide metapopulation dynamics supports a pathway to extinction that began long before the Holocene, when the combination of cooling temperatures and low but sustained hunting by humans trapped woolly rhinoceroses in suboptimal habitats along the southern edge of their range. Modeling indicates that this ecological trap intensified after the end of the last ice age, preventing colonization of newly formed suitable habitats, weakening stabilizing metapopulation processes, triggering the extinction of the woolly rhinoceros in the early Holocene. Our findings suggest that fragmentation and resultant metapopulation dynamics should be explicitly considered in explanations of late Quaternary megafauna extinctions, sending a clarion call to the fragility of the remaining large-bodied grazers restricted to disjunct fragments of poor-quality habitat due to anthropogenic environmental change.

megafauna | metapopulation dynamics | ecological mechanisms | synergistic interactions | reconstructing extinctions

Significance

Using a computationally intensive modeling approach and extensive paleontological and ancient DNA information, we reveal how and why the woolly rhinoceros went extinct at a fine spatiotemporal resolution. Our population reconstructions indicate that a combination of climate-driven habitat fragmentation and low but persistent levels of hunting by humans weakened metapopulation processes and caused their extinction. Our results provide a deeper understanding of the structure and dynamics of past extinctions of megafauna, simultaneously providing valuable lessons to safeguard Earth's remaining large animals.

Population processes and their spatial dynamics (1–3) have rarely been considered as critical determinants of late Quaternary extinctions of megafauna, with efforts instead being largely directed to understanding the relative roles of climatic change and human impacts, or their synergy, on the timing and rate of extinctions (4–8). This partly reflects current difficulties in determining important mechanistic responses of late Quaternary megafauna to causal drivers of demographic change at fine spatiotemporal resolutions exclusively using available genetic and paleontological techniques (9). Evidence for causation, therefore, tends to be highly uncertain, and even conflicting, leading to fierce debates regarding putative drivers of late Quaternary extinctions and their synergistic interactions (10–12). A more comprehensive exploration of the demographic, genetic, climatic, and anthropogenic causes of megafaunal collapse is therefore needed to better establish the ecological processes and spatiotemporal threats that were integral in the decline of extinct late Quaternary megafauna. These insights, in turn, should provide salient lessons to conserve Earth's remaining large wildlife.

Process-explicit models provide powerful approaches for detecting determinants of extinctions across space and time (13). When integrated with distribution and demographic information from fossils and ancient DNA, they can identify the most likely dynamics of ancient extinctions at high spatiotemporal resolutions (9, 14). Clues to chains of causality can be identified from these reconstructions of population decline and extinction, including assessments of independent and potentially interactive effects of natural and anthropogenic forces on vital demographic and genetic processes (9, 14). Nevertheless, previous attempts to tease apart various putative drivers of population and range declines of extinct megafauna have mainly used correlative and not mechanistic techniques (6, 7, 15), thus limiting our understandings of the metapopulation processes and dynamics responsible for the fates of lost megafauna (13).

The woolly rhinoceros (*Coelodonta antiquitatis*) was an iconic member of the mammoth steppe (16) fauna of central and northern Eurasia (15), originating on the Tibetan

plateau approximately 2.5 million years ago (17). It was a cold-adapted species covered in thick skin and long fur, with a body size similar to the extant African white rhinoceros (*Ceratotherium simum*) (18). Based on fossil chronology, the woolly rhinoceros was presumed extinct by the onset of the warm and wet Allerød oscillation ~13.9 thousand B.P. (ka B.P.), despite surviving repeated glacial-interglacial cycles of the Pleistocene (15). However, the recent discovery of woolly rhinoceros DNA in early Holocene sediments indicates a later extinction date of ~9.8 ka B.P. While there is ongoing debate surrounding this young age estimate (19), redeposition of DNA is unlikely to be its cause (20).

Dentition patterns and stomach content analysis point toward the woolly rhinoceros being a grazer, feeding on low vegetation growing in dry open landscapes (18). Wear-patterns from subfossils indicate that it probably used its front horn to expose herbaceous vegetation in shallow snow (17). Radiocarbon-dated fossils show that the woolly rhinoceros was distributed across northern Eurasia until ~35 ka B.P., when it experienced a progressive eastward range contraction during the late Pleistocene (15). It has been hypothesized that climate-driven environmental change and an ecological preference of woolly rhinoceroses for dry-open landscapes with low snow cover were the principal causes of their decline and later extinction (15). This was postulated partly because, although cold-adapted, the woolly rhinoceros had short bulky legs without spreading hooves or pads, which would have made moving through deep snow that formed after the last ice age difficult (18), potentially increasing the susceptibility of populations to human impacts (5).

There remains, however, much debate regarding the extrinsic causes of decline of the woolly rhinoceros, the potential roles of humans, the timing of its extinction, and the population processes and dynamics leading to its extinction. Mitochondrial DNA sequence data retrieved from woolly rhinoceros subfossils indicate a fivefold increase in population size at the onset of the last glacial maximum (LGM) at ~26 ka B.P. (7). This is also supported by nuclear DNA, which additionally shows an abrupt—almost instantaneous—extinction of the woolly rhinoceros in response to rapid warming at the termination of the Pleistocene (6). However, the woolly rhinoceros survived past glacial-interglacial transitions, some more severe than the last (21), only to vanish in the interglacial period where modern humans were first present. This included persisting through the Eemian (~130 to 115 ka B.P.), when temperatures in Europe were generally warmer than those of the 20th century (22). Resolving this discrepancy between inferences of progressive extinction based on fossils and abrupt extinction based on DNA, could benefit from a more thorough (process-based) investigation of how climatic change and human pressures directly or synergistically affected the ecology and demography of the woolly rhinoceros, causing its extinction.

Here, we assess the ecological mechanisms and threats that are likely to have been integral to population declines and the extinction of the woolly rhinoceros from 60 ka B.P. at a spatiotemporal resolution higher than that of previous studies. We did this by simulating 45,000 plausible spatially explicit scenarios of process-driven interactions among woolly rhinoceroses, climate, and humans. We optimized model parameters with pattern-oriented methods (23) using ecological inferences from hundreds of high-quality radiocarbon dated fossils (Dataset S1) and independently validated these models using available ancient DNA retrieved from sediments (20). Our 52,000-y continuous reconstruction of distribution-wide metapopulation dynamics points toward a pathway to extinction that began long before the Last Glacial Maximum, when cooling temperatures and low but constant hunting by humans trapped woolly rhinoceroses in isolated, suboptimal habitats along the southern edge of their range.

Results and Discussion

The simulation models of climate–human–woolly rhinoceros interactions that could accurately reconstruct fossil evidence of the decline and extinction of the woolly rhinoceros (occurrence at fossil sites, timings of regional extirpation, and absence in North America; Fig. 1) converged on highly constrained parameters. This indicates that the woolly rhinoceros is likely to have had a broad realized ecological niche, low population abundance, and a limited capacity for dispersal (*SI Appendix*, Fig. S1 and Table S1). These "best models" (the 0.2 % of all models that most closely hit the validation targets) suggest a pathway to extinction that began long before the LGM, when cooling temperatures and human hunting disrupted metapopulation dynamics, ultimately leading to population declines (Fig. 2) and a southward range contraction, confining woolly rhinoceroses to isolated fragments of suboptimal climatic habitat. In the few locations (mainly the oldest and most southern fossil sites) where our models projected timing of extirpation to have occurred earlier than expected from paleontological data (Fig. 1), they correctly projected persistence close to these fossil sites (Movie S1).

Extinction Dynamics. Our modeling indicates that the woolly rhinoceros did indeed experience an on-going eastward contraction of its distribution from ~35 ka B.P. (onset of the GI-7 interstadial), and this range contraction and population decline accelerated as climatic conditions warmed—causing higher precipitation and snowfall (25)—following GIS-3 (23.3 ka B.P.) and the most recent ice age (Fig. 2 and Movie S1). From the onset of the Holocene (~11.7 ka B.P.), the woolly rhinoceros is likely to have persisted primarily in Siberia, finally going extinct in north-east Siberia at ~8.7 ka B.P. (Fig. 1) due to interactions between changes in local environmental conditions, deteriorating metapopulation processes, and human impacts (Fig. 3). This timing and location of extinction closely matches independent evidence from ancient sedimentary DNA (Fig. 1).

Reconciling inferences of demographic change from the fossil chronology in process-explicit simulations required the woolly rhinoceros to become trapped in suboptimal climatic habitat at the end of the Pleistocene, and to persist from this time onward in a scattering of isolated populations (Fig. 3). From as early as ~33 ka B.P., our results suggest that some populations of the woolly rhinoceros failed to utilize large adjoining patches of highly suitable habitat during periods of rapid environmental change (Movie S2). This is despite them being intermittently connected to occupied populations by corridors of seasonally suitable, but snow-covered habitat.

Populations of the woolly rhinoceros are likely to have continued to decline during the early Holocene, because of climate-driven environmental change (Fig. 4) and its negative impact on habitat quality and connectivity among populations (Fig. 3). By 9.7 ka B.P., the strength of vital metapopulation processes most likely weakened, because populations of the woolly rhinoceros were so few and isolated from each other that demographic rescue (3) from source-type populations could no longer occur (Fig. 3). Environmental and demographic stochastic processes in these disconnected and small populations probably strengthened, causing population-level fitness to decline (1), ultimately triggering extinction. This was despite persistence and expansion of extensive areas of suitable, but now isolated, habitat during the early Holocene (Fig. 3).
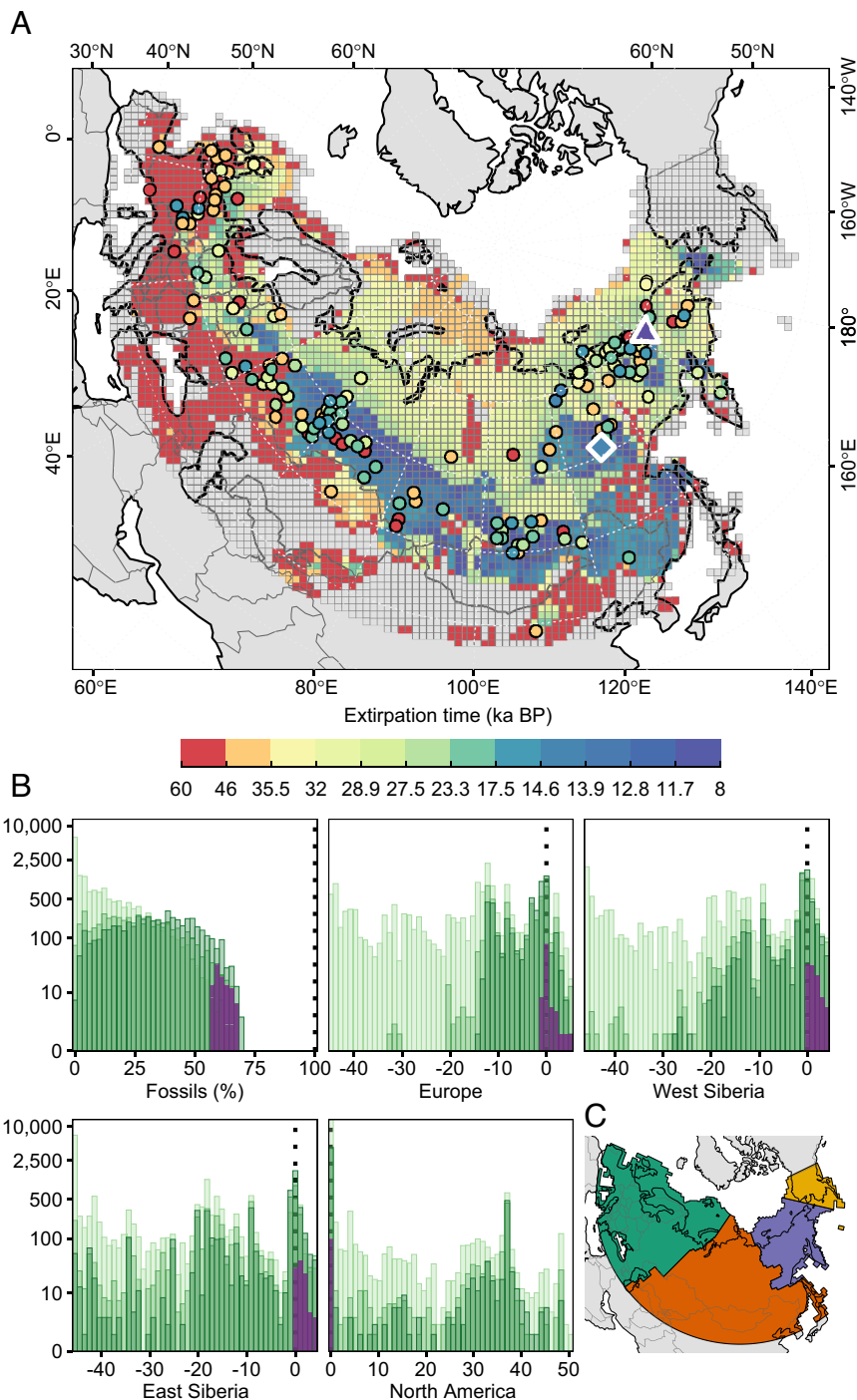
Fig. 1. Timing of woolly rhinoceros extirpation across Eurasia. (*A*) Grid-cell colors on the map show simulated time of extirpation. Circles show fossil locations, with colors representing the youngest age estimate (mean age + 1 SD). The blue diamond shows the youngest radiocarbon dated woolly rhinoceros fossil. The purple triangle shows youngest estimate of occurrence from sedimentary ancient DNA (20). Gray cells were never occupied. (*B*) Histograms shows the ability of process-driven models to correctly project spatiotemporal occurrence at fossil sites, displayed as a percentage (Fossil %); estimate timing of regional extinction in Europe, West Siberia, and East Siberia, shown as difference in years (kyr); and period of occupancy in North America, also shown in years (kyr). Validation targets are displayed as dotted black lines. Purple colored bars show selected models. Green colored bars show all models; shades of green represent different rounds of pattern-oriented modeling, with lighter colors representing earlier rounds. *Inset* map (*C*) shows the regions: Europe (green), west Siberia (orange), east Siberia (purple), and North America (yellow).

Causal Drivers. Anatomically modern humans arrived in Eurasia as early as 55 ka B.P., spreading to many of its most remote and extreme environments by 45 ka B.P. (26). Here, woolly rhinoceroses co-occurred with modern humans for tens of thousands of years, and Neanderthals (*Homo neanderthalensis*) and other hominins for even longer, where they exploited woolly rhinoceroses and other wildlife for food (27). Although hunting has so far not

been considered an important driver of population decline or extinction of the woolly rhinoceros (6, 7, 15), isotopic analysis suggests that the species comprised up to 30% of the protein intake for humans in some areas of Eurasia (28). Accordingly, our 52,000-y reconstruction of spatial population processes and abundances of the woolly rhinoceros indicates that hunting of this species by humans is likely to have played an important,
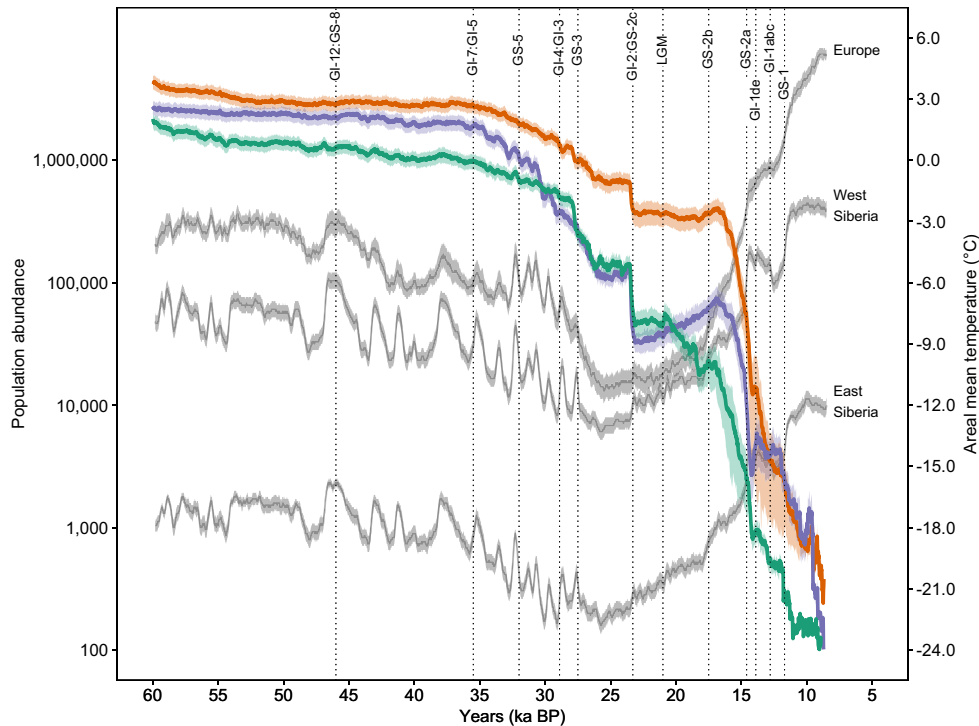
Fig. 2. Abundance of woolly rhinoceroses across 52,000 y. Total population abundances (on a log-scale) for Europe (green), west Siberia (orange), and east Siberia (purple). Gray lines show the areal annual mean temperature for each region. Shaded areas show the 95% CI. Dotted lines indicate the boundaries of major stadial/interstadials (24). Regional boundaries are shown in Fig. 1.

albeit, largely overlooked role in its decline (Fig. 4), with humans removing an average of 10% (SD = 5%) of woolly rhinoceros populations per generation.

Prior to the LGM, densities of humans are most likely to have been relatively high in areas along the southern distribution of the woolly rhinoceros (*SI Appendix*, Fig. S2). Here, our modeling suggests that hunting at levels typically less than that for other mammoth steppe fauna (*SI Appendix*, Table S1)—including woolly mammoth (9) and steppe bison (14)—contributed to declines in population abundances of woolly rhinoceroses (Fig. 4 and *SI Appendix*, Fig. S3). In north-eastern Siberia and northern Europe, where human densities were typically lower (averaging < 2 % of densities at the southern extent of the woolly rhinoceros' distribution; *SI Appendix*, Fig. S2) (29), our results, using paleoclimate simulations, point toward temperature and snow cover as being more dominant factors regulating population abundances of the woolly rhinoceros during this time period (Fig. 4 and *SI Appendix*, Figs. S4 and S5).

Following the LGM, our modeling indicates that temperature and snow depth drove the largest changes in population abundances across the entire remaining distribution of the woolly rhinoceros (Fig. 4). While interactive effects of humans on population abundances of woolly rhinoceroses are likely to have remained secondary to climatic factors for the rest of its existence, they were vital for extinction. Paleontological evidence suggests that humans hunted woolly rhinoceroses during the last deglaciation (28), and our simulations show that low levels of hunting after (as well as before) the LGM are critical to reconstruct the extinction of the woolly rhinoceros in the early Holocene (*SI Appendix*, Figs. S3 and S6).

Proximate impacts of climatic warming during the Pleistocene–Holocene transition are likely to have largely stemmed from resultant shifts in vegetation composition across Eurasia, which affected food availability for grazers, as well as other trophic groups (16, 20). Our modeling shows that these climate-driven changes probably

weakened metapopulation structures (Movie S1), making the woolly rhinoceros potentially more susceptible to human impacts (5). From 14.6 to 12.8 ka B.P., woolly rhinoceroses were generally found at highest abundance in south-east Siberia (Movie S1) where smaller increases in winter snow depth (Fig. 4 and *SI Appendix*, Figs. S5–S7) probably enabled food to be more readily accessible and dispersal among populations to be higher. Temperatures continued to rise across Eurasia after 12.8 ka B.P. (GS-1; Fig. 2) (24), with larger temperature increases in southern Siberia compared to northern Siberia (*SI Appendix*, Fig. S8), likely causing more severe declines in abundances in southern populations (Movie S1). Cooler and drier Holocene conditions in north-east Siberia (*SI Appendix*, Figs. S8 and S9) favored preferred graminoid and forb tundra (25), prolonging range-wide persistence of the woolly rhinoceros in those regions (7). While regulation of plant structure and biomass by herbivores during the Pleistocene has been suggested, its importance remains uncertain (30, 31), making it a fertile topic for future research using our modeling technique.

Hindcasting our validated model of climate–human–woolly rhinoceros interactions back to the Eemian, when temperatures were similar to today (22), indicated a wide distribution for the woolly rhinoceros at 120 ka B.P. (*SI Appendix*, Fig. S10), owing to its broad ecological tolerance (*SI Appendix*, Fig. S11) and the absence of anatomically modern humans. Bayesian sensitivity analysis of posterior model parameters (32) confirmed that woolly rhinoceroses had a wide ecological tolerance (*SI Appendix*, Table S1). It also showed that reconciling inferences of range collapse and extinction from fossils and ancient DNA requires low and sustained levels of hunting by humans. Importantly, hindcasts at the most recent interglacial, provide evidence that our simulations appropriately captured the upper warm tolerance of woolly rhinoceroses in climate-driven ecological responses, including those identified as critical for the extinction of the woolly rhinoceros in the early Holocene.
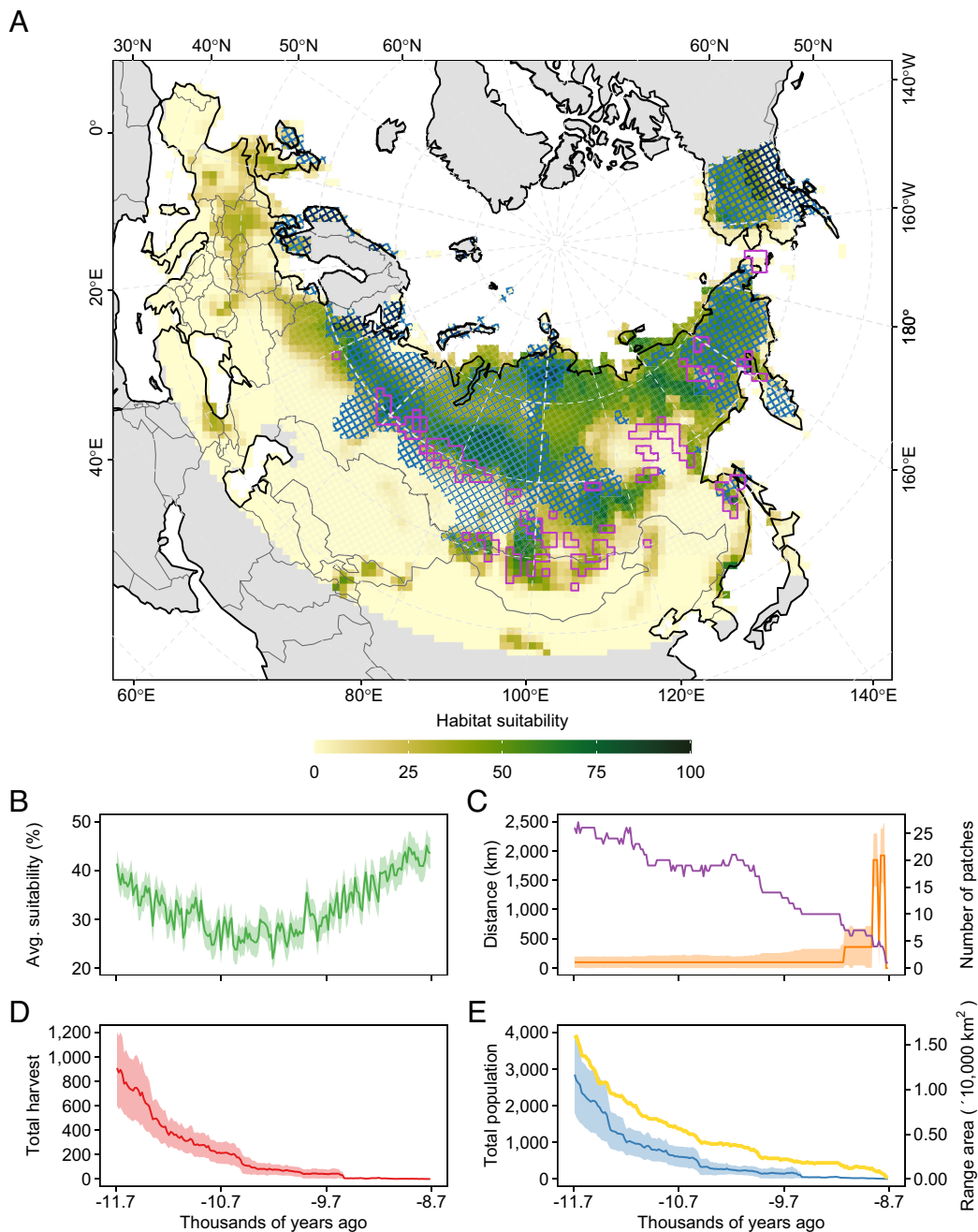
Fig. 3. Drivers of final woolly rhinoceros extinction in the Holocene. (*A*) Map shows mean habitat suitability for the early Holocene (from 11.7 to 8.7 ka BP), with purple areas indicating patches of habitat that were occupied at any time during this period. Hatched areas indicate areas of moderate (0.6 to 1.5 m, blue) and deep (>1.5 m, black) winter snow. (*B*) Habitat suitability, (*C*) average minimum distance between patches (orange line) and number of patches (purple line), (*D*) total harvest offtake, and (*E*) total population size (blue line) and range area (yellow line) for habitats occupied during the Holocene (purple cells in *A*). Shaded areas in (*B*–*E*) represent the 95% CI.

Spatial Population Processes. Disruption of metapopulation dynamics has rarely been directly considered in explanations of late Quaternary megafauna extinctions, despite having the potential to cause devastating effects on the persistence of species at landscape scales (33). This is somewhat surprising, given previous suggestions that metapopulation processes, including the weakening of source-sink dynamics (2), and the establishment of ecological traps (33, 34), have heightened the risk of extinction for extant relatives of the woolly rhinoceros (34–36). Our modeling shows that reconciling available paleontological data, and their inferences, requires complex interactions between climate change, human activities, and population processes of woolly rhinoceroses, causing their range to contract to isolated, suboptimal climatic habitats at the end of the last ice age (Movie S1). It also indicates that

otherwise stabilizing source–sink dynamics weakened during the Pleistocene–Holocene transition, ultimately leading to extinction in the early Holocene (Fig. 3).

Evidence that populations of woolly rhinoceroses failed to colonize highly suitable climatic habitats from ~33 ka B.P., despite there being putative corridors for dispersal, can be attributed potentially to a combination of high energy costs associated with moving through deep winter snow (18), and impacts of human populations on dispersing woolly rhinoceroses (*SI Appendix,* Fig. S2). Modeling indicates that the formation of such ecological traps intensified following the LGM, when climatic conditions changed rapidly, preventing northward migrations to suitable areas, including the Taymyr peninsula. Thus, the woolly rhinoceros was trapped in the southern (trailing) edge of its contracting
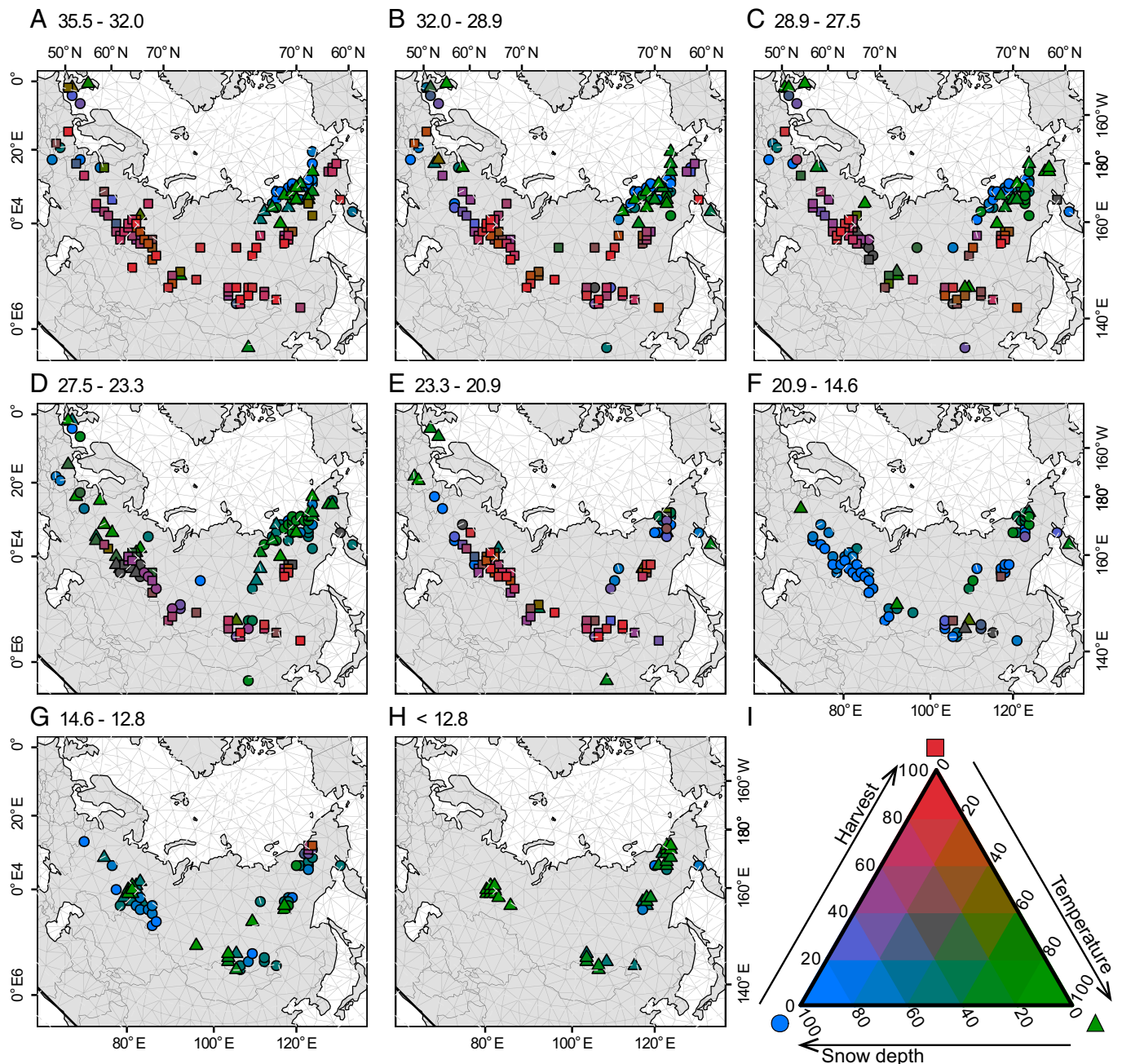
Fig. 4. Spatiotemporal variation in woolly rhinoceros extinction drivers. Maps show the contributing effects of annual mean temperature (green triangles), annual mean snow depth (blue circles), and relative human harvest (red squares) on site-level abundance through space and time. Periods in (*A–H*) are shown as years ka B.P. Colors in the spectral diagram (*I*) show the relative strength of the three drivers. Maps of coefficient estimates for individual drivers and spatiotemporal random effects are shown in *SI Appendix*, Figs. S3, S4, S5, and S13.

range, and this probably led to its eventual extinction thousands of years later (Movie S1).

Furthermore, our modeling confirms that a low capacity for dispersal is likely to have contributed to woolly rhinoceroses not crossing the Bering Strait and colonizing suitable climatic habitat in North America. Long-distance dispersal rates, generally less than 150 km per generation (*SI Appendix*, Fig. S12), were needed to reconstruct the absence of woolly rhinoceroses in North America, as well as other validation metrics (occurrence at fossil sites, and timings of regional extirpation). This supports previous suggestions that a morphology not suited for movement over long distances, particularly through wet boggy habitat, prevented woolly rhinoceroses from crossing the Bering Land Bridge and colonizing the New World (15, 30).

Differences remain between the extinction timeline and dynamics uncovered here using our process-driven modeling approach, and those inferred previously from ancient DNA retrieved from macrofossils (6, 7). These dissimilarities probably arise because the demographic responses captured in our analysis are at a higher spatiotemporal resolution than those in previous genetic studies. A relative scarcity of high-quality ancient DNA data from the woolly rhinoceros has precluded the direct consideration of important dynamic interactions between spatial demographic processes and extrinsic factors in past genetic estimates of its population change. These include humans weakening dispersal and recolonization processes of the woolly rhinoceros during the late Pleistocene, causing increased vulnerability to climatic warming in the Holocene due to deteriorating regulatory metapopulation processes.

While our results mechanistically reconstructed the likely pattern of range contraction and extinction of the woolly rhinoceros in accordance with independent evidence from ancient DNA analysis of sediments (Fig. 1), this additional verification of our results was done with few samples, including only one from the early Holocene (20). Looking ahead, we expect that the precision of our simulations of the spatiotemporal abundance of the woolly rhinoceros, and its timing and location of extinction, will continue to improve with further fossil discoveries, more extensive ancient DNA analysis of sediments, projections of human population growth and migration that account for topographical processes and cultural changes in Eurasia, and improved paleoclimatic simulations of rainfall and snowfall.

Our finding that climate-driven habitat fragmentation and low but persistent levels of hunting by humans are likely to have synergistically weakened metapopulation processes, causing the decline and ultimate extinction of the woolly rhinoceros, has strong conservation implications. Most remaining megafauna persist in a tiny fraction of their historical range due to an insidious combination of land-use change and human hunting (35). Sixty-one terrestrial megaherbivores ≥1,000 kg existed during the late Pleistocene (37), however, only eight such species survive today. Five are rhinoceroses, four of which are endangered, three critically (38).

Today, rhinoceroses persist in highly fragmented ranges across Africa and Asia. On both continents, they are generally found only in isolated, suboptimal habitats (36), many of which are forecast to experience rapid climate-driven decline and further fragmentation over the coming decades (39). Low dispersal capacities, confounded by anthropogenic dispersal barriers and poaching, severely threaten these remaining charismatic and irreplaceable megafaunas, with issues of increased inbreeding and genetic load already written in their genomes (40). Without enhanced conservation efforts, these extant species will continue to find themselves trapped in suboptimal habitats, isolated and unable to respond to climatic warming, as the woolly rhinoceros once did, following a similar fate.

Materials and Methods

Process-driven statistical-simulation models of climate–human–woolly rhinoceros interactions, which integrate extensive palaeoecological information, were developed to reconstruct critical interactions between intrinsic demographic processes and extrinsic environmental factors that caused the decline and extinction of the woolly rhinoceros (13). Pattern-oriented modeling techniques (23) and Approximate Bayesian Computation (41) were used to identify vital processes, find accurate parameters, and validate models (42).

Niche Estimation. Radiocarbon dated and georeferenced fossils of woolly rhinoceroses from the Late Pleistocene and Holocene were sourced from publicly accessible databases and published literature (*SI Appendix, Materials and Methods*). Their reliability was assessed using a numeric ranking based on the Mead-Meltzer scale, updated to reflect advances in radiocarbon dating and to better incorporate archeological evidence (43). All reliable fossils were age-calibrated using OxCal (44) and the IntCal13 calibration curve (45).

The HadCM3B-M2.1 coupled general circulation model (GCM) was used to generate monthly climatic parameters from 60 ka B.P. to the present (1950 CE) (46) at a resampled resolution of 1°×1° (*SI Appendix, Materials and Methods*). Tests show that the model reproduces an accurate representation of land and sea temperatures, precipitation, and ocean circulation (47). We intersected fossil locations and time periods (calibrated age ± 1 SD) with paleosimulations of climatic parameters (temperature, precipitation, evapotranspiration) that are likely to have affected the population dynamics of the woolly rhinoceros and characterized an n-dimensional hypervolume of climatic suitability through time (9). The resulting hypervolume, which represents the full potential climatic niche of the woolly rhinoceros (48), was exhaustively subsampled to derive its realized niche using process-driven statistical-simulation techniques (see below). By capturing

occurrence climate relationships at fossil sites through time, including periods when modern humans were low in abundance in Eurasia (*SI Appendix*, Fig. S2), this multitemporal ecological niche modeling approach limited any niche truncation (49).

Spatial projections of climate suitability for the woolly rhinoceros in Eurasia were generated from 60 ka B.P. to 8 ka B.P. at 17-y (generational) time steps for each plausible realized niche ($n = 3,000$ subsamples of the full hypervolume of climate suitability). We used a Lambert Azimuthal Equal Area projection centered on 104° east and 60° north, with a resolution of 100 km × 100 km. A projection of climatic suitability was also made for the Eemian (130 to 15 ka B.P.). See *SI Appendix, Materials and Methods* for further information on the fossil data and projections of climate suitability.

Humans. The peopling of Eurasia, and their relative abundances, were modeled using the climate informed spatial genetic model (CISGeM), which accurately reconstructs the arrival times of anatomically modern humans and contemporary distributions of global and regional genetic diversity (50, 51). Recently, it has been coupled to macroecological models to establish megafauna–human interactions (9, 14). Local effective population size (N_e) is simulated in CISGeM as a function of net primary productivity (NPP), genetic history, and local demography.

CISGeM was used to calculate a time-series of relative local population change for humans from 120 ka B.P. to 0 B.P. at 25-y time steps. Arrival, occupancy, and density (N_e) were forced by spatiotemporal estimates of climate and sea level changes over the past 125 k y using HadCM3B-M2.1 GCM. To account for parameter uncertainty in spatiotemporal projections of N_e, we ran 4,900 unique models (each with different parameter settings) using established model parameters (50). N_e values were then scaled between 0 and 1 using the 95th percentile of maximum values and used in the process-driven climate–human–woolly rhinoceros interaction model as potential spatiotemporal measures of relative abundance of humans. CISGeM and its application are described in detail in *SI Appendix, Materials and Methods*.

Climate–Human–Woolly Rhinoceros Interactions. Metapopulation dynamics were simulated as landscape-level population processes for the woolly rhinoceros, operating at a 17-y generational time steps from 60 ka B.P. Models centered on best estimates for demographic processes (population growth rate and variance, dispersal proportion and distance, Allee effect), environmental attributes (niche breadth, climatic specialization), and human interactions (human abundance, rates of exploitation, functional response) were varied across plausible ranges using Latin hypercube sampling, to provide a robust coverage of multidimensional parameter space (9). This procedure produced 45,000 conceivable models (i.e., individual parameterizations) with different combinations of demographic processes, environmental affinities, and climate and human impacts. Each model was run for a single replicate (52). The structure and parameters of the process-driven model of climate–human–woolly rhinoceros interactions are described in detail in *SI Appendix, Materials and Methods*.

Pattern-oriented modeling (23) was used to evaluate different conceivable model parameterizations, by cross matching simulations with inferences of underlying population dynamics from paleoarchives, using Approximate Bayesian Computation (41). Specifically, simulations of metapopulation dynamics and their driving forces were validated against a five-parameter multivariate target, which characterized patterns of range collapse and extinction of the woolly rhinoceros observed from the fossil record at multiple scales. Bayes factors and posterior-predictive checks were used to detect when the posterior parameters had converged. The top 100 feasible parameterizations (0.22 %) of climate–human–woolly rhinoceros interactions were able to reconstruct occurrence at fossil sites at the correct time (^{14}C age ± 1 SD), accurately predict the timing of regional extinction events (corrected for the Signor–Lipps effect; (53)), and project a distribution restricted to Eurasia (15). These "best" models were retained and used to generate weighted ensemble averaged estimates of spatial abundance, extirpation time, total population size, population fragmentation, and harvest rates. Estimates were weighted by inverse of the Euclidean distance of the model from the idealized targets, giving higher weights to models that best reproduced our validation targets. Further validation of the selected models was then done using independent estimates of extirpation inferred from ancient sedimentary DNA (20).

Statistical Analysis. Bayesian linear models (32) were used to identify which model parameters had the largest influence on minimizing the Euclidian distance between simulated and inferred demographic change. Models were constructed with uniform priors ($\beta_k \sim R2(0.5)$) and 10 chains, each with 50,000 samples, with the first 10,000 samples being discarded as burn-in. We ensured model convergence using Gelman–Rubin statistics (where values less than or equal to 1.1 were considered acceptable), tested for effective sample size, and visually examined trace-plots. We quantified the existence, significance, and size of the effect of each parameter using a Bayesian effects framework (54).

To disentangle the spatiotemporal processes and drivers that caused the extinction of the woolly rhinoceros, we extracted a time series of abundance and harvest rate (from our validated process-driven simulation model) at each geographic location where a woolly rhinoceros fossil has been found and reliably radiocarbon dated, starting at 60 ka B.P. This information was matched with a time series of modeled annual average temperatures and annual average snow depths (46) for each site. Spatiotemporal generalized linear mixed-effects models were used to quantify spatiotemporal determinants of abundance from 60 ka B.P. for 12 distinct glacial/interglacial periods (15) using the sdmTMB package for R (55). Harvest, temperature, snow depth, and year were modeled as main effects, with spatially varying intercepts and coefficients for the first three variables. Regression coefficients were used to explain dominant drivers leading to population declines and extinction of woolly rhinoceroses. Statistical analyses are described in more detail in *SI Appendix, Materials and Methods*.

Eemian Hindcast. We tested whether our process-driven modeling approach could reconstruct the persistence of woolly rhinoceroses during Pleistocene interglacial events that they had previously survived. This was done by simulating best estimates of climate–human–woolly rhinoceros interactions (based on pattern-oriented modeling) under climate and environmental conditions at 120 ka B.P.–a snapshot of Eemian conditions. While close-range hunting of woolly rhinoceroses by Neanderthals is likely, it was not considered in these simulations because of high uncertainty in spatiotemporal abundances of early hominids and their hunting strategies (56). Moreover, these simulations did not account for important ecological and spatiotemporal processes leading into the Eemian, making their projections of range and abundance, somewhat optimistic (9). This includes projections of persistence in low densities in what are likely to have been densely forested habitats at the last interglacial.

Author affiliations: [a]The Environment Institute, School of Biological Sciences, University of Adelaide, Adelaide SA, 5005, Australia; [b]Center for Macroecology, Evolution, and Climate, Globe Institute, University of Copenhagen, Copenhagen Ø 2100, Denmark; [c]Center for Global Mountain Biodiversity, Globe Institute, University of Copenhagen, Copenhagen Ø 2100, Denmark; [d]Globe Institute, University of Copenhagen, Copenhagen K 1350, Denmark; [e]Department of Environmental and Forest Biology, College of Environmental Science, Syracuse, NY 13210; [f]Centre of Excellence for Biosecurity Risk Analysis, School of Biosciences, University of Melbourne, Melbourne, VIC 3010, Australia; [g]Department of Geosciences and Geography, University of Helsinki, Helsinki, FI-00014, Finland; [h]Senckenberg Centre for Human Evolution and Palaeoenvironment, Tübingen 72074, Germany; [i]Department of Geosciences, Biogeology, University of Tübingen, Tübingen 72074, Germany; [j]Department of Zoology, University of Cambridge, CB23EJ Cambridge, United Kingdom; [k]Institute of Ecology, Peking University, Beijing 100871, China; and [l]Danish Institute for Advanced Study, University of Southern Denmark, Odense M 5230, Denmark

1. R. Lande, Risks of population extinction from demographic and environmental stochasticity and random catastrophes. *Am. Nat.* **142**, 911–927 (1993).
2. I. Hanski, Patch-occupancy dynamics in fragmented landscapes. *Trends Ecol. Evol.* **9**, 131–135 (1994).
3. R. A. Hufbauer et al., Three types of rescue can avert extinction in a changing environment. *Proc. Natl. Acad. Sci. U.S.A.* **112**, 10557–10562 (2015).
4. A. D. Barnosky, P. L. Koch, R. S. Feranec, S. L. Wing, A. B. Shabel, Assessing the causes of late pleistocene extinctions on the continents. *Science* **306**, 70–75 (2004).
5. A. Cooper et al., Abrupt warming events drove Late Pleistocene Holarctic megafaunal turnover. *Science* **349**, 602–606 (2015).
6. E. Lord et al., Pre-extinction demographic stability and genomic signatures of adaptation in the woolly rhinoceros. *Curr. Biol.* **30**, 3871–3879.e3877 (2020).
7. E. D. Lorenzen et al., Species-specific responses of Late Quaternary megafauna to climate and humans. *Nature* **479**, 359–364 (2011).
8. F. A. Smith, R. E. Elliott Smith, S. K. Lyons, J. L. Payne, Body size downgrading of mammals over the late Quaternary. *Science* **360**, 310–313 (2018).
9. D. A. Fordham et al., Process-explicit models reveal pathway to extinction for woolly mammoth using pattern-oriented validation. *Ecol. Lett.* **25**, 125–137 (2022).
10. S. Wroe et al., Climate change frames debate over the extinction of megafauna in Sahul (Pleistocene Australia-New Guinea). *Proc. Natl. Acad. Sci. U.S.A.* **110**, 8777–8781 (2013).
11. F. Saltré et al., Climate change not to blame for late Quaternary megafauna extinctions in Australia. *Nat. Commun.* **7**, 10511 (2016).
12. J. L. Metcalf et al., Synergistic roles of climate warming and human occupation in Patagonian megafaunal extinctions during the Last Deglaciation. *Sci. Adv.* **2**, e1501682 (2016).
13. J. Pilowsky, R. K. Colwell, C. Rahbek, D. A. Fordham, Process-explicit models reveal the structure and dynamics of biodiversity patterns. *Sci. Adv.* **8**, eabj2271 (2022), 10.1126/sciadv.abj2271.
14. J. A. Pilowsky et al., Range and extinction dynamics of the steppe bison in Siberia: A pattern-oriented modeling approach. *Global Ecol. Biogeogr.* **31**, 2483–2497 (2022), 10.1111/geb.13601.
15. A. J. Stuart, A. M. Lister, Extinction chronology of the woolly rhinoceros Coelodonta antiquitatis in the context of late Quaternary megafaunal extinctions in northern Eurasia. *Q. Sci. Rev.* **51**, 1–17 (2012).
16. E. Willerslev et al., Fifty thousand years of Arctic vegetation and megafaunal diet. *Nature* **506**, 47–51 (2014).
17. R.-D. Kahlke, F. Lacombat, The earliest immigration of woolly rhinoceros (Coelodonta tologoijensis, Rhinocerotidae, Mammalia) into Europe and its adaptive evolution in Palaearctic cold stage mammal faunas. *Q. Sci. Rev.* **27**, 1951–1961 (2008).
18. G. G. Boeskorov, Some specific morphological and ecological features of the fossil woolly rhinoceros (Coelodonta antiquitatis Blumenbach 1799). *Biol. Bull.* **39**, 692–707 (2012).
19. J. H. Miller, C. Simpson, When did mammoths go extinct? *Nature* **612**, E1–E3 (2022).
20. Y. Wang et al., Late Quaternary dynamics of Arctic biota from ancient environmental genomics. *Nature* **600**, 86–92 (2021).
21. J. R. Petit et al., Climate and atmospheric history of the past 420,000 years from the Vostok ice core, Antarctica. *Nature* **399**, 429–436 (1999).
22. F. Kaspar, N. Kühl, U. Cubasch, T. Litt, A model-data comparison of European temperatures in the Eemian interglacial. *Geophys. Res. Lett.* **32**, L11703 (2005).
23. V. Grimm et al., Pattern-oriented modeling of agent-based complex systems: Lessons from ecology. *Science* **310**, 987–991 (2005).
24. S. O. Rasmussen et al., A stratigraphic framework for abrupt climatic changes during the Last Glacial period based on three synchronized Greenland ice-core records: Refining and extending the INTIMATE event stratigraphy. *Q. Sci. Rev.* **106**, 14–28 (2014).
25. H. Binney et al., Vegetation of Eurasia from the last glacial maximum to present: Key biogeographic patterns. *Q. Sci. Rev.* **157**, 80–97 (2017).
26. V. V. Pitulko et al., Early human presence in the Arctic: Evidence from 45,000-year-old mammoth remains. *Science* **351**, 260–263 (2016).
27. H. Bocherens, "Diet and ecology of Neanderthals: Implications from C and N isotopes" in *Neanderthal Lifeways, Subsistence and Technology: One Hundred Fifty Years of Neanderthal Study*, N. J. Conard, J. Richter, Eds. (Springer, Netherlands, Dordrecht, 2011), pp. 73–85, 10.1007/978-94-007-0415-2_8.
28. C. Wißing et al., Stable isotopes reveal patterns of diet and mobility in the last Neandertals and first modern humans in Europe. *Sci. Rep.* **9**, 4433 (2019).
29. L. Pagani et al., Genomic analyses inform on migration events during the peopling of Eurasia. *Nature* **538**, 238–242 (2016).
30. R. Dale Guthrie, Origin and causes of the mammoth steppe: A story of cloud cover, woolly mammal tooth pits, buckles, and inside-out Beringia. *Q. Sci. Rev.* **20**, 549–574 (2001).
31. D. Zhu et al., The large mean body size of mammalian herbivores explains the productivity paradox during the Last Glacial Maximum. *Nat. Ecol. Evol.* **2**, 640–649 (2018).
32. S. R. Coutts, H. Yokomizo, Meta-models as a straightforward approach to the sensitivity analysis of complex models. *Popul. Ecol.* **56**, 7–19 (2014).
33. R. Hale, E. A. Treml, S. E. Swearer, Evaluating the metapopulation consequences of ecological traps. *Proc. R. Soc. B: Biol. Sci.* **282**, 20142930 (2015).
34. N. le Roex, C. Dreyer, S. M. Ferreira, Poaching creates ecological traps within an iconic protected area. *Anim. Conserv.* **23**, 250–259 (2020).
35. W. J. Ripple et al., Collapse of the world's largest herbivores. *Sci. Adv.* **1**, e1400103 (2015).
36. R. Amin, K. Thomas, R. H. Emslie, T. J. Foose, N. V. Strien, An overview of the conservation status of and threats to rhinoceros species in the wild. *Int. Zoo Yearbook* **40**, 96–117 (2006).
37. Y. Malhi et al., Megafauna and ecosystem function from the Pleistocene to the Anthropocene. *Proc. Natl. Acad. Sci. U.S.A.* **113**, 838–846 (2016).
38. IUCN, The IUCN Red List of Threatened Species. Version 2022-1. https://www.iucnredlist.org. Accessed 10 July 2022.
39. M. F. Kinnaird, E. W. Sanderson, T. G. O'Brien, H. T. Wibisono, G. Woolmer, Deforestation trends in a tropical landscape and implications for endangered large mammals. *Conserv. Biol.* **17**, 245–257 (2003).
40. S. Liu et al., Ancient and modern genomes unravel the evolutionary history of the rhinoceros family. *Cell* **184**, 4874–4885.e4816 (2021).
41. K. Csilléry, M. G. Blum, O. E. Gaggiotti, O. Francois, Approximate Bayesian Computation (ABC) in practice. *Trends Ecol. Evol.* **25**, 410–418 (2010).
42. S.C. Brown, D.A. Fordham, Woolly rhinoceros extinction dynamics computational code. OSF. https://osf.io/6f5md/. Accessed 14 September 2023.
43. A. D. Barnosky, E. L. Lindsey, Timing of quaternary megafaunal extinction in South America in relation to human arrival and climate change. *Q. Int.* **217**, 10–29 (2010).
44. C. Bronk Ramsey, Bayesian analysis of radiocarbon dates. *Radiocarbon* **51**, 337–360 (2016).
45. P. J. Reimer et al., Intcal13 and Marine13 radiocarbon age calibration curves 0–50,000 years Cal BP. *Radiocarbon* **55**, 1869–1887 (2013).

46. E. Armstrong, P. O. Hopcroft, P. J. Valdes, A simulated Northern Hemisphere terrestrial climate dataset for the past 60,000 years. *Sci. Data* **6**, 265 (2019).
47. P. J. Valdes *et al.*, The BRIDGE HadCM3 family of climate models: HadCM3@Bristol v1.0. *Geosci. Model Dev.* **10**, 3715–3743 (2017).
48. D. Nogués-Bravo, Predicting the past distribution of species climatic niches. *Glob. Ecol. Biogeogr.* **18**, 521–531 (2009).
49. S. Faurby, M. B. Araujo, Anthropogenic range contractions bias species climate change forecasts. *Nat. Clim. Change* **8**, 252-+ (2018).
50. A. Eriksson *et al.*, Late Pleistocene climate change and the global expansion of anatomically modern humans. *Proc. Natl. Acad. Sci. U.S.A.* **109**, 16089–16094 (2012).
51. M. Raghavan *et al.*, Genomic evidence for the Pleistocene and recent population history of Native Americans. *Science* **349**, aab3884 (2015).
52. T. A. A. Prowse *et al.*, An efficient protocol for the global sensitivity analysis of stochastic ecological models. *Ecosphere* **7**, e01238 (2016).
53. P. W. Signor, J. H. Lipps, "Sampling bias, gradual extinction patterns and catastrophes in the fossil record" in *Geological Implications of Impacts of Large Asteroids and Comets on the Earth*, L. T. Silver, P. H. Schultz, Eds. (Geological Society of America, 1982), **vol. 190**, pp. 291–296.
54. D. Makowski, M. S. Ben-Shachar, S. H. A. Chen, D. Lüdecke, Indices of effect existence and significance in the Bayesian framework. *Front. Psychol.* **10**, 2767 (2019).
55. S. C. Anderson, E. J. Ward, P. A. English, L. A. K. Barnett, sdmTMB: An R package for fast, flexible, and user-friendly generalized linear mixed effects models with spatial and spatiotemporal random fields. bioRxiv [Preprint] (2022). https://doi.org/10.1101/2022.03.24.485545 (Accessed 8 May 2023).
56. S. Gaudzinski-Windheuser *et al.*, Evidence for close-range hunting by last interglacial Neanderthals. *Nat. Ecol. Evol.* **2**, 1087–1092 (2018).